Longitudinal and transverse components of excitons in a spherical quantum dot

Hiroshi Ajiki and Kikuo Cho
Department of Physical Science, Graduate School of Engineering Science, Osaka University, Toyonaka, Osaka 560-8531, Japan
(Received 17 February 2000)

Exciton states confined in a spherical quantum dot (QD) are studied in a weak confinement regime with the consideration of the electron-hole exchange interaction and induced surface charge density. Except for special cases, most exciton states are longitudinal (L)–transverse (T) mixed modes. With an increase of radius, the LT mixed modes approach bulk L, T, and surface (S) modes. When the energies of LT mixed modes get close to that of the S mode, they acquire considerable amount of S-mode character. It is demonstrated that the effect of the surface charge density does not affect the L-mode exciton confined in an arbitrary shape. Within the long-wavelength approximation, one-photon transitions toward the pure L and T modes are forbidden, and for other states the oscillator strengths per unit volume become maximum around the energy of the S mode.

I. INTRODUCTION

Recently, exciton states confined in a zero-dimensional microcrystal, which is usually called quantum dot (QD), have been investigated extensively. Various QD's embedded in glasses[1,2] and in alkali-halide crystals[3–9] have been grown. The optical properties of these QD's have been studied mainly in the aspect of the quantum-size effect of optically excited electron-hole (e-h) pairs. The effect manifests itself as blue shifts of absorption and luminescence peaks.

The motion of an e-h pair is quite different in two limiting situations characterized by the ratio of the QD's size R_Q to the effective Bohr radius a_B of an exciton in bulk material.[10] The energy of an e-h pair is mainly determined by the individual size quantization with a small correction due to the Coulomb interaction in the case of $R_Q \ll a_B$ (strong-confinement regime). In the opposite situation $R_Q \gg a_B$ (weak-confinement regime), the e-h relative motion stays almost as in the bulk and only the center-of-mass (c.m.) motion is affected by the confinement. The evolution of an e-h pair state from strong- to weak-confinement regime has been studied via variational methods based on effective-mass theory.[11–16]

It is well known that excitons in a bulk crystal have longitudinal (L) and transverse (T) characters according to its polarization direction with respect to the translational wave vector. (In the absence of translational symmetry as in QD's, the definition of the L and T modes can be generalized as $\mathrm{rot}\,\mathbf{P}=\mathbf{0}$ and $\mathrm{div}\,\mathbf{P}=0$, respectively.) In high-symmetry crystals, the L and T characters are kept in the exciton dispersion curves. When the exciton is confined, the boundary condition for its wave function leads to a set of discrete allowed wave vectors on the dispersion curve. The problem is whether the boundary condition can be applied to the L and T branches separately or not, but it is hard to find any evident reason that allows it. Theoretically, it has not been made clear whether the same level scheme occurs in a QD as in the bulk with respect to the L and T level arrangement. However, an experimental work claims or suggests the existence of LT splitting in a QD as in the bulk.[17]

Some theoretical studies on spherically confined excitons have been made, including the e-h exchange interaction,[16,18–20] but they are not enough to answer the question mentioned above. In considering the LT splitting or the effect of e-h exchange interaction, there are two different viewpoints. In one case, (a) this interaction is considered as a part of matter energy, and in the other, (b) it is considered to be the interaction energy between the matter polarization density and (external) longitudinal electric field. In each scheme, the definition of the matter Hamiltonian, susceptibility tensors, and electromagnetic (em) field as a source of matter polarization is different. The relationship between the two schemes has recently been discussed by one of the authors,[21] who pointed out how these two schemes are connected via the e-h exchange interaction. The works of Ruppin[19] and Ekimov *et al.*[18] are based on scheme (b), and those by Takagahara[16] and Goupalov and Ivchenko[20] belong to scheme (a).

In scheme (b), one calculates the optical response by solving Maxwell equations with a given susceptibility and assuming an additional boundary condition for connecting em field across the boundary of confinement. The resonant structure reflects the level scheme of the QD, but every level is shifted and broadened from the corresponding level scheme (a) due to the interaction with transverse em field. From the optical spectrum, it is hard to tell the L and T characters of each resonant level.

For the study of the level structure in scheme (a), we start from a general expression of the applicable e-h exchange interaction, not only to the bulk crystals, but also to QD's. It was demonstrated[21] that the use of the induced charge density (off-diagonal matrix element of charge-density operator, or -div of the induced polarization) for each size-quantized exciton state is the most general way until now to express the effect of LT splitting. The Coulomb interaction of these induced charge densities coincides with the e-h exchange matrix element, and this form can be directly applied to both bulk and confined systems and also to both phonons and excitons. Our study in this paper is based on scheme (a) together with the modeling of the induced charge densities for size-quantized excitons appropriate for the weak-confinement regime.

As another point of this work, we include the effect of nonresonant polarization in QD and its surrounding materi-

als. There are many other polarizations in the system, which are usually treated as a background dielectric medium in considering exciton resonances. If one treats only the resonant modes as dynamical variables, the effect of nonresonant modes can be taken into account by multiplying a screening constant $1/\epsilon_b$ to Coulomb interaction energy. For a finite-size system, however, we need an additional consideration of the induced surface charge density due to the polarization of the background dielectric (i.e., the assembly of nonresonant modes). This mirror-charge or image-potential effect modifies the e-h attraction energy and the e-h exchange interaction among the resonant modes. The effect of the e-h binding was studied by Brus[11] and Takagahara,[16] but the image-potential effect on the latter problem has not been studied. The effect of the bulklike screening of the e-h exchange was considered in our previous work[22] but the image-potential effect was neglected. The present work is a revised version of our previous paper in this respect.

The present calculation shows the results of diagonalizing the size-quantized kinetic energy of exciton c.m. motion and the e-h exchange interaction among the resonant exciton levels, with due consideration of the image-potential effect. The radius of the sphere is changed in the weak-confinement regime up to infinity. Due to spherical symmetry, all the levels are classified according to the total angular momentum and its projection. Except for special cases, most levels have LT mixed character in general. As the radius gets larger, these levels tend to converge to those of L, T, and S (surface) modes of the corresponding bulk system. The effect of the image potential shifts the energy of the S mode, but not those of T and L modes in the bulk limit. For finite radius, the mixing of L, T, and S modes occurs in general.

This paper is organized as follows: In Sec. II we provide an effective-mass equation of c.m. motion confined in arbitrary shape, including the e-h exchange interaction and image potential. In Sec. III the equation is applied to the spherical confinement case, and we will find some excitons to be pure L and T modes independent of confinement size. Analytical results of exciton states with infinite mass are obtained in Sec. IV. In Sec. V the states of finite-mass exciton are calculated numerically. The L and T characters and oscillator strengths per unit volume are discussed. A summary and conclusion are given in Sec. VI.

The level structure obtained from the present study is just that of the matter system. How it is reflected in the optical spectrum must be calculated in the next step. From the viewpoint of scheme (a), this calculation is appropriately done with the help of microscopic nonlocal theory of optical response developed by us.[23–25] The result is planned to be published in the near future. A preliminary account of this work has been presented elsewhere.[26]

II. ELECTRON-HOLE INTERACTION IN A CONFINED MEDIUM

Here we derive the effective-mass equation for the c.m. motion of an exciton confined in a QD in the weak confinement regime, including the e-h exchange interaction and image-potential effect. We assume that the system consists of a background dielectric and a number of electrons contributing to the formation of the exciton states. The effect of the background dielectric is considered in the Hamiltonian of these electrons. In general, the image-potential energy coming from more than one charged particle is divided into two parts, i.e., the energy of image potential induced by itself and other charged particles. We describe the former ''self-energy'' part as $q^2U_{\rm im}$ and the latter part as $q^2V_{\rm im}$. Then, the Hamiltonian is written as

$$
\begin{aligned}
H=&\sum_l \left[-\frac{\hbar^2\nabla_l^2}{2m_e}+W(\mathbf{r}_l)+W_c(\mathbf{r}_l)\right]+\tfrac{1}{2}\sum_{l\neq l'}\sum \frac{1}{\epsilon_1}\frac{q^2}{|\mathbf{r}_l-\mathbf{r}_{l'}|}\\
&+\sum_l q^2U_{\rm im}(\mathbf{r}_l)+\tfrac{1}{2}\sum_{l\neq l'}\sum q^2V_{\rm im}(\mathbf{r}_l,\mathbf{r}_{l'})\\
&+\Bigg[\sum_i q^2U_{\rm im}(\mathbf{R}_i)-\sum_l\sum_i q^2V_{\rm im}(\mathbf{r}_l,\mathbf{R}_i)\\
&+\tfrac{1}{2}\sum_{i\neq j}\sum q^2V_{\rm im}(\mathbf{R}_i,\mathbf{R}_j)\Bigg],
\end{aligned}
\tag{2.1}
$$

where l indicates electron index, m_e the mass of electron, W the periodic potential by the crystal, W_c the confinement potential of QD, ϵ_1 the background dielectric constant of QD, and $\mathbf{R}_i$ the position of periodic positive ions. The last three terms are the image-potential energies of positive ions, which ensures, in the case of charge neutrality, that the overall image potential becomes zero in the ground state.

The conduction and valence bands will be denoted by ν and μ, respectively, each of which includes a spin quantum number. The wave function of one exciton state can be described by

$$
\Psi=\sum_{\nu\mu}\sum_{ij} F_{\nu\mu}(\mathbf{R}_i,\mathbf{R}_j)\Phi_{ij}^{\nu\mu}, \tag{2.2}
$$

where $\Phi_{ij}^{\nu\mu}$ is the Slater determinant of the configuration in which an electron of a Wannier state $\phi_\mu(\mathbf{r}-\mathbf{R}_j)$ is excited into $\phi_\nu(\mathbf{r}-\mathbf{R}_i)$, and $F_{\nu\mu}(\mathbf{R}_i,\mathbf{R}_j)$ is the normalized envelope function associated with the Slater determinant.

Using the fact that a Wannier function $\phi_{\mu(\nu)}(\mathbf{r}-\mathbf{R})$ is well localized around an atomic site $\mathbf{R}$, we obtain the Schrödinger equation for the envelope function giving the excitation energy E' from the ground state as follows:

$$
\sum_{\nu'\mu'}\sum_{i'j'} H^{ij,i'j'}_{\nu\mu,\nu'\mu'}F_{\nu'\mu'}(\mathbf{R}_{i'},\mathbf{R}_{j'})=E'F_{\nu\mu}(\mathbf{R}_i,\mathbf{R}_j), \tag{2.3}
$$

with

$$H^{ij,i'j'}_{\nu\mu,\nu'\mu'}=\left\{\varepsilon_c(-i\nabla_i)-\varepsilon_v(-i\nabla_j)-\frac{q^2}{\epsilon_1}\frac{1}{|\mathbf{R}_i-\mathbf{R}_j|}+W_c(\mathbf{R}_i)\right.$$
$$+W_c(\mathbf{R}_j)+q^2[U_{\rm im}(\mathbf{R}_i)+U_{\rm im}(\mathbf{R}_j)$$
$$\left.-V_{\rm im}(\mathbf{R}_i,\mathbf{R}_j)]\right\}\delta_{\nu\nu'}\delta_{\mu\mu'}\delta_{ii'}\delta_{jj'}$$
$$+\int d\mathbf{r}\int d\mathbf{r}'\,\rho^*_{\nu\mu}(\mathbf{r}-\mathbf{R}_i)\left[\frac{1}{\epsilon_1}\frac{1}{|\mathbf{r}-\mathbf{r}'|}\right.$$
$$\left.+V_{\rm im}(\mathbf{r},\mathbf{r}')\right]\rho_{\nu'\mu'}(\mathbf{r}'-\mathbf{R}_{i'})\delta_{ij}\delta_{i'j'}, \tag{2.4}$$

where ε_c and ε_v are the energies of the conduction and valence bands, respectively, and $\rho_{\nu\mu}$ is the matrix element of charge-density operator between the ground state and $\Phi^{\nu\mu}_{ij}$, i.e.,

$$\rho_{\nu\mu}(\mathbf{r}-\mathbf{R}_i)=q\,\phi^*_\nu(\mathbf{r}-\mathbf{R}_i)\,\phi_\mu(\mathbf{r}-\mathbf{R}_i). \tag{2.5}$$

The last term in Eq. (2.4) originates from the *e-h* exchange interaction,[27–29] and it has the form of the Coulomb interaction between induced charge densities $\rho_{\nu\mu}$. The induced charge density takes a finite value only for the same spin states of ν and μ (spin-singlet *e-h* pair) as a result of the inner product for spin states. In the following, we will consider only the spin-singlet exciton and regard μ and ν as band indices excluding spin states. Note that the expression of the *e-h* exchange interaction in terms of the induced charge densities is an exact and model-independent one, from which one can derive ''short- and long-range parts'' or ''analytic and nonanalytic parts'' of the *e-h* exchange interaction. In the following model of this paper, we use a smooth form of the induced charge density of a confined exciton, which is equivalent to neglecting analytic part of the *e-h* exchange interaction.

For Wannier sites with larger distances than the extension of Wannier functions, one can expand $1/|\mathbf{r}-\mathbf{r}'|$ to obtain the *e-h* exchange part $H_{\rm exch}$ in terms of induced polarization as follows:

$$H_{\rm exch}=\boldsymbol{\mu}^*_{\nu\mu}\cdot\left[\nabla_i\nabla_{i'}\left(\frac{1}{\epsilon_1}\frac{1}{|\mathbf{R}_i-\mathbf{R}_{i'}|}\right.\right.$$
$$\left.\left.+V_{\rm im}(\mathbf{R}_i,\mathbf{R}_{i'})\right)\right]\cdot\boldsymbol{\mu}_{\nu'\mu'}\delta_{ij}\delta_{i'j'}, \tag{2.6}$$

where $\boldsymbol{\mu}_{\nu\mu}$ is the induced polarization given by

$$\boldsymbol{\mu}_{\nu\mu}=\int d\mathbf{r}\,\rho_{\nu\mu}(\mathbf{r})\mathbf{r}. \tag{2.7}$$

In our previous work to estimate the image-potential energy of *e-h* exchange interaction for exciton states in a spherical QD, we introduced a virtual spherical boundary of dielectric constants and calculated the work to shrink the boundary from infinity to the QD's radius.[26] However, this procedure is incorrect because the *e-h* exchange interaction arises from the Coulomb interaction between different electrons, as explicitly shown in the last terms of Eq. (2.4).

In the weak-confinement regime the envelope function of an exciton is approximately separated into the relative and c.m. motions. In this regime the image potential in the *e-h* attraction terms do not affect the relative motion considerably.[16] The confinement potential is assumed to be infinite, and we apply the boundary condition that the wave function of c.m. motion vanishes at the effective confinement boundary. Furthermore, we approximate that the wave function of the relative motion is the same as that in a bulk crystal. Considering the simplest model of direct band gap at the band center with isotropic effective masses, we obtain the equation satisfying the c.m. motion in the effective-mass approximation as follows:

$$\sum_{\nu'\mu'}\int d\mathbf{r}'[\phi(0)\boldsymbol{\mu}_{\nu\mu}]^*\cdot\left\{\nabla\nabla'\left[\frac{1}{\epsilon_1}\frac{1}{|\mathbf{r}-\mathbf{r}'|}\right.\right.$$
$$\left.\left.+V_{\rm im}(\mathbf{r},\mathbf{r}')\right]\right\}\cdot[\phi(0)\boldsymbol{\mu}_{\nu'\mu'}]G_{\nu'\mu'}(\mathbf{r}')$$
$$-\frac{\hbar^2}{2M_{\rm ex}}\nabla^2G_{\nu\mu}(\mathbf{r})=EG_{\nu\mu}(\mathbf{r}), \tag{2.8}$$

where $M_{\rm ex}$ is the transnational mass, $G_{\nu\mu}$ and ϕ are the wave function of the c.m. and relative motions, respectively, and E is the energy measured from the excitation energy toward the transverse exciton at band center in a bulk crystal. We have approximated that the envelope function $G_{\nu\mu}$ does not change over the range of effective Bohr radius, and the electron or hole position is replaced by the position of c.m. motion in the *e-h* exchange term.

Finally we obtain matrix elements of the Hamiltonian

$$H_{\nu\mu,\nu'\mu'}=-\frac{\hbar^2}{2M_{\rm ex}}\int d\mathbf{r}\,G^*_{\nu\mu}(\mathbf{r})\nabla^2G_{\nu'\mu'}(\mathbf{r})$$
$$+\int d\mathbf{r}\int d\mathbf{r}'[-\nabla\cdot\mathbf{P}_{\nu\mu}(\mathbf{r})]^*\left[\frac{1}{\epsilon_1}\frac{1}{|\mathbf{r}-\mathbf{r}'|}\right.$$
$$\left.+V_{\rm im}(\mathbf{r},\mathbf{r}')\right][-\nabla\cdot\mathbf{P}_{\nu'\mu'}(\mathbf{r}')], \tag{2.9}$$

with

$$\mathbf{P}_{\nu\mu}(\mathbf{r})=\boldsymbol{\mu}_{\nu\mu}\phi(0)G_{\nu\mu}(\mathbf{r}), \tag{2.10}$$

where we have integrated by parts with respect to $\mathbf{r}$ and $\mathbf{r}'$ in the *e-h* exchange term. The resulting *e-h* exchange term corresponds to the nonanalytic part giving the *L-T* splitting energy in bulk systems. The intensity of the induced polarization $\mu=|\boldsymbol{\mu}_{\mu\mu}\phi(0)|$ is obtained from the bulk limit. Substituting the polarization of the bulk L mode $\mathbf{P}(\mathbf{r})=\boldsymbol{\mu}\exp(i\mathbf{k}\cdot\mathbf{r})/\sqrt{V}$, where V is volume and $\boldsymbol{\mu}$ is parallel to $\mathbf{k}$, into the *e-h* exchange interaction without the image potential in Eq. (2.9), we get

$$\mu^2=\frac{\epsilon_1\Delta_{LT}}{4\pi} \tag{2.11}$$

where Δ_{LT} is the splitting energy of L and T modes of exciton.

III. EXCITON IN A SPHERICAL QUANTUM DOT

A. Set of bases

We consider an exciton in a spherical QD with radius a and dielectric constant ϵ_1 that is embedded in an isotropic continuous medium with dielectric constant ϵ_2. The crystal forming the QD is assumed to have either the valence or conduction band with s-like character and the other with p-like character that possesses three degenerate states p_x, p_y, and p_z. In this case three possible combinations of $(\nu\mu)$ give the three transition-dipole moments $\boldsymbol{\mu}_{\nu\mu}$, each of which is polarized in the x, y, and z direction, and thus the combinations of band indices can be indicated by the unit vectors $\mathbf{e}_x$, $\mathbf{e}_y$, and $\mathbf{e}_z$. In the following we will use three-dimensional vector functions without band indices as a set of bases.

In spherical coordinates, it is useful to introduce the vector functions given in terms of the vector spherical harmonics $\mathbf{Y}_{J\ell M}(\hat{\mathbf{r}})$ as follows:

$$\mathbf{Q}_{nJ\ell M}=\sqrt{\frac{2}{a^3}}\frac{j_\ell(k_{n\ell}r)}{J_{\ell+1}(\kappa_{n\ell})}\mathbf{Y}_{J\ell M}(\hat{\mathbf{r}}), \tag{3.1}$$

where $j_\ell(x)$ is the spherical Bessel function of order ℓ, and $k_{n\ell}=k_{n\ell}a$ is the nth zero of $j_\ell(x)$. The discrete wave numbers $k_{n\ell}$ are chosen to satisfy the boundary condition.

The vector spherical harmonics is the eigenfunction of the added angular momentum of ℓ and ℓ' ($|\ell'|=1$) relating to the unit polarization vector[30]

$$\mathbf{Y}_{J\ell M}(\hat{\mathbf{r}})=\sum_{m=-\ell}^{1}\sum_{s=-1}^{1}\langle \ell m 1s|\ell 1JM\rangle Y_{\ell m}(\hat{\mathbf{r}})\mathbf{e}_s, \tag{3.2}$$

where $\langle \ell m 1s|\ell 1JM\rangle$ is the Clebsch-Gordan coefficient, $Y_{\ell m}(\hat{\mathbf{r}})$ is the spherical harmonics with $\hat{\mathbf{r}}$ being the angular variable, and $\mathbf{e}_s$ are the spherical unit vectors

$$\mathbf{e}_{\pm1}=\mp\frac{1}{\sqrt{2}}(\mathbf{e}_x\pm i\mathbf{e}_y),\quad \mathbf{e}_0=\mathbf{e}_z. \tag{3.3}$$

The quantum numbers J and M are the total angular momentum and its projection, respectively. For $J\geqslant 1$, ℓ itself runs from $J-1$ to $J+1$, and for $J=0$ the allowed value of ℓ is only 1.

The vector functions $\mathbf{Q}_{nJ\ell M}(\mathbf{r})$ form an orthonormal set

$$\int d\mathbf{r}\,\mathbf{Q}^*_{nJ\ell M}(\mathbf{r})\cdot\mathbf{Q}_{n'J'\ell'M'}(\mathbf{r})=\delta_{nn'}\delta_{JJ'}\delta_{\ell\ell'}\delta_{MM'}, \tag{3.4}$$

and the set is complete. Furthermore, the bases are the eigenfunctions of the kinetic part, whose matrix elements are given by

$$H^{\rm kin}_{\xi\xi'}=\frac{\hbar^2k^2_{n\ell}}{2M_{\rm ex}}\delta_{\xi\xi'}, \tag{3.5}$$

where ξ represents a set of quantum numbers (n,J,ℓ,M).

B. Electron-hole exchange energy

In a confinement system e-h exchange interaction consists of ''direct'' and image-potential terms, which correspond to the first and the second terms of the induced polarization interaction in Eq. (2.9), respectively. For our model the induced polarization is written as $\mathbf{P}_\xi=\mu\mathbf{Q}_\xi$ where μ is the intensity of polarization given in Eq. (2.11), and the polarization charge density is obtained from

$$\boldsymbol{\nabla}\cdot\mathbf{Q}_{nJ\ell M}(\mathbf{r})=-k_{n\ell}P_{J\ell}\sqrt{\frac{2}{a^3}}\frac{j_J(k_{n\ell}r)}{j_{\ell+1}(\kappa_{n\ell})}Y_{JM}(\hat{\mathbf{r}}), \tag{3.6}$$

with

$$P_{J\ell}=\begin{cases}\sqrt{\dfrac{J}{2J+1}} & (\ell=J-1),\\ 0 & (\ell=J),\\ \sqrt{\dfrac{J+1}{2J+1}} & (\ell=J+1).\end{cases} \tag{3.7}$$

The ''direct'' term is calculated as

$$\begin{aligned}H^{\rm dir}_{\xi\xi'}&=\int d\mathbf{r}\int d\mathbf{r}'[-\boldsymbol{\nabla}\cdot\mathbf{P}_\xi(\mathbf{r})]^*\frac{1}{\epsilon_1}\frac{1}{|\mathbf{r}-\mathbf{r}'|}[-\boldsymbol{\nabla}'\cdot\mathbf{P}_{\xi'}(\mathbf{r}')]\\&=\delta_{JJ'}\delta_{MM'}\Delta_{LT}\\&\quad\times\begin{cases}P^2_{J\ell}\delta_{nn'} & (\ell=\ell'),\\ \sqrt{J(J+1)}f_{nn'J} & (\ell=J+1,\ \ell'=J-1),\\ \sqrt{J(J+1)}f_{n'nJ} & (\ell=J-1,\ \ell'=J+1),\end{cases}\end{aligned} \tag{3.8}$$

with

$$f_{nn'J}=\frac{2\kappa_{nJ+1}}{\kappa_{n'J-1}(\kappa^2_{nJ+1}-\kappa^2_{n'J-1})}. \tag{3.9}$$

In the above calculation we have used the expansion

$$\frac{1}{|\mathbf{r}-\mathbf{r}'|}=\sum_{\ell=0}^{\infty}\sum_{m=-\ell}^{\ell}\frac{4\pi}{2\ell+1}\frac{r^\ell_<}{r^{\ell+1}_>}Y_{\ell m}(\hat{\mathbf{r}})Y^*_{\ell m}(\mathbf{r}'), \tag{3.10}$$

where $r_>$ is the larger of r and r' and $r_<$ is the smaller of r and r', and the integral formula

$$\int_0^1 dx \int_0^1 dx' x^2 x'^2 \frac{x_<^\ell}{x_>^{\ell+1}} J_\ell(\alpha x) j_\ell(\beta x)$$

$$= \begin{cases} \dfrac{2\ell+1}{\beta^2(\alpha^2-\beta^2)}[\alpha j_{\ell+1}(\alpha) j_\ell(\beta) - \beta j_\ell(\alpha) j_{\ell+1}(\beta)] - \dfrac{j_{\ell+1}(\alpha) j_{\ell-1}(\alpha)}{\alpha^2} & (\alpha \neq \beta), \\ \dfrac{2\ell+1}{2\alpha^3}[\alpha\{j_\ell^2(\alpha) + j_{\ell+1}^2(\alpha)\} - (2\ell+1) j_\ell(\alpha) j_{\ell+1}(\alpha)] - \dfrac{j_{\ell+1}(\alpha) j_{\ell-1}(\alpha)}{\alpha^2} & (\alpha = \beta). \end{cases} \tag{3.11}$$

It should be noted that, for given good quantum numbers J and M, $\ell = J-1$ and $\ell = J+1$ states are mixed via $H^{\rm dir}$. Namely, for $J=1$, $\ell=0$ and $\ell=2$ states are mixed. This conclusion seems to be inconsistent with that of Takagahara, where the long-range part makes no contribution to the exciton levels.[16] This is because he was interested in the strong-confinement regime alone, though his wave function has a general form applicable to both strong- and weak-confinement regimes. The mixing scheme mentioned above applies to both strong- and weak-confinement regimes. For the discussion about the effect of LT splitting in this paper, it is crucial to consider both $\ell = J-1$ and $\ell = J+1$ subspaces.

For spherical shape the image potential in the Hamiltonian equation (2.1) is given by[11]

$$U_{\rm im}(\mathbf{r}) = \frac{1}{2}\frac{1}{\epsilon_1}\sum_\ell \frac{(\ell+1)(1-\bar{\epsilon})}{\ell+\bar{\epsilon}(\ell+1)} \frac{r^{2\ell}}{a^{2\ell+1}},$$

$$U_{\rm im}(\mathbf{r},\mathbf{r}') = \frac{1}{\epsilon_1}\sum_\ell \frac{(\ell+1)(1-\bar{\epsilon})}{\ell+\bar{\epsilon}(\ell+1)} \frac{r^\ell r'^l}{a^{2\ell+1}} P_\ell(\cos\theta), \tag{3.12}$$

where $\bar{\epsilon} = \epsilon_2/\epsilon_1$ is the relative dielectric constant and $P_\ell(\cos\theta)$ is the Legendre polynomial with θ being the angle between $\mathbf{r}$ and $\mathbf{r}'$. Thus the e-h exchange energy coming from image-potential effect is obtained as

$$H^{\rm im}_{\xi\xi'} = \int d\mathbf{r} \int d\mathbf{r}' [-\nabla\cdot\mathbf{P}_\xi(\mathbf{r})]^* V_{\rm im}(\mathbf{r},\mathbf{r}') [-\nabla'\cdot\mathbf{P}_{\xi'}(\mathbf{r}')]$$

$$= \gamma(\bar{\epsilon},J) \frac{1}{\kappa_{nJ-1}\kappa_{n'J-1}} \Delta_{LT}\delta_{JJ'}\delta_{MM'}\delta_{\ell J-1}\delta_{\ell' J-1}, \tag{3.13}$$

with

$$\gamma(\bar{\epsilon},J) = 2\frac{(1-\bar{\epsilon})J(J+1)}{\bar{\epsilon}(J+1)+J}. \tag{3.14}$$

The image-potential energy depends on the relative dielectric constant. When the dielectric constants inside and outside of the sphere are the same ($\bar{\epsilon}=1$), the matrix elements of the image potential become zero. For $\epsilon_1 > \epsilon_2$ ($\epsilon_1 < \epsilon_2$) the image-potential energy becomes positive (negative). In usual experiments ϵ_2 is smaller than ϵ_1, and thus the image potential raises the energy of confined exciton.

C. Pure L and T modes

The exciton levels in a sphere are obtained from diagonalizing the Hamiltonian

$$H_{\xi\xi'} = H^{\rm kin}_{\xi\xi'} + H^{\rm dir}_{\xi\xi'} + H^{\rm im}_{\xi\xi'}, \tag{3.15}$$

which has a block-diagonalized form with respect to J and M because of spherical symmetry. In some cases eigenstates of an exciton are obtained immediately, and these states are found to be L or T mode independent of the size of sphere.

By definition, the rotation of L-mode polarization and the divergence of T-mode polarization are zero everywhere. Otherwise, a polarization is a LT mixed mode. It is useful to provide the divergence and rotation of a set of $\{\mathbf{Q}_\xi\}$ to investigate the L- or T-mode character of spherically confined exciton. The divergence of $\mathbf{Q}_\xi$ is given in Eq. (3.6) and the rotation is

$$\nabla\times\mathbf{Q}_{nJJM}(\mathbf{r}) = -k_{nJ}\sqrt{\frac{2}{a^3}}\frac{1}{j_{J+1}(\kappa_{nJ})} \times \sum_{\ell=J-1,J+1} \bar{P}_{J\ell} j_\ell(k_{nJ}r)\mathbf{Y}_{J\ell M}(\hat{\mathbf{r}}),$$

$$\nabla\times\mathbf{Q}_{nJ\ell M}(\mathbf{r}) = k_{n\ell}\bar{P}_{J\ell}\sqrt{\frac{2}{a^3}}\frac{j_J(k_{n\ell}r)}{j_{\ell+1}(\kappa_{n\ell})}\mathbf{Y}_{JJM}(\hat{\mathbf{r}}), \tag{3.16}$$

with

$$\bar{P}_{J\ell} = \begin{cases} -i\sqrt{\dfrac{J+1}{2J+1}} & (\ell = J-1) \\ i\sqrt{\dfrac{J}{2J+1}} & (\ell = J+1) \end{cases}. \tag{3.17}$$

For $J=\ell\geq 1$, $P_{J\ell}=0$ and for $J=0$, $\bar{P}_{J\ell}=0$. Thus the former (latter) is pure T (L) mode, and its energy is $(\hbar^2 k_{nJ}^2/2M_{\rm ex})(\hbar^2 k_{nJ}^2/2M_{\rm ex}+\Delta_{LT})$.

IV. THE CASE OF INFINITE MASS

Let us consider the case without spatial dispersion, i.e., the kinetic part of the Hamiltonian is neglected. The situation occurs for infinitely large translational mass of exciton. In this limit we can calculate exciton levels analytically.

First, we confine ourselves to the subspace $\ell = J-1$. Then the Schrödinger equation is written as

$$\Delta_{LT}\sum_m \left[\frac{J}{2J+1}\delta_{nm}+\frac{\gamma(\bar{\epsilon},J)}{\kappa_{nJ-1}\kappa_{mJ-1}}\right]C_{mJ-1}=EC_{nJ-1}, \tag{4.1}$$

where $C_{n\ell}$ is the expansion coefficient with respect to the basis $\mathbf{Q}_{nj\ell M}$. Multiplying Eq. (4.1) by κ_{nJ-1}^{-1} and summing over n, we have

$$\Delta_{LT}\left[\frac{J}{2J+1}+\gamma(\bar{\epsilon},J)\sum_n \kappa_{nJ-1}^{-2}\right]X=EX, \tag{4.2}$$

with $X=\Sigma_n\kappa_{nJ-1}^{-1}C_{nJ-1}$. The solution of Eq. (4.2) turns out to be of the S mode as will be shown later, and its energy is

$$E_J^{\rm surf}=\frac{J}{J+(J+1)\bar{\epsilon}}\Delta_{LT}. \tag{4.3}$$

The corresponding eigenstates are

$$\mathbf{Q}_{JM}^{\rm surf}(\mathbf{r})=\sqrt{2(2J+1)}\sum_n \kappa_{nJ-1}^{-1}\mathbf{Q}_{nJJ-1M}(\mathbf{r})$$
$$=\sqrt{\frac{2J+1}{a^3}}r^{J-1}\mathbf{Y}_{JJ-1M}, \tag{4.4}$$

where we have used Eq. (A1) in the Appendix. The resulting energy is the same as that obtained from dielectric function and Maxwell's boundary conditions.[31]

We now choose a complete set of bases $\{\mathbf{Q}_{JM}^{\rm surf},\mathbf{Q}_{JM}^{Am},\mathbf{Q}_{JM}^{Bm}\}$ for given J and M, as

$$\mathbf{Q}_{JM}^{Am}(\mathbf{r})=(2J+1)\sum_n f_{mnJ}\mathbf{Q}_{nJJ-1M}(\mathbf{r}),$$
$$\mathbf{Q}_{JM}^{Bm}(\mathbf{r})=\mathbf{Q}_{mJJ+1M}. \tag{4.5}$$

The bases form an orthonormal set, which is confirmed by using Eqs. (A1)–(A4) in the Appendix, and the Hamiltonian is represented in the bases as follows:

$$\mathbf{Q}_{JM}^{\rm surf}\begin{pmatrix} E_J^{\rm surf} & 0 & & & \\ 0 & K & 0 & & \\ & 0 & K & 0 & \\ & & \ddots & \ddots & \ddots \end{pmatrix}, \tag{4.6}$$

with

$$K=\begin{matrix}\mathbf{Q}_{JM}^{Am}\\ \mathbf{Q}_{JM}^{Bm}\end{matrix}\begin{pmatrix} P_{JJ-1}^2 & P_{JJ-1}P_{JJ+1} \\ P_{JJ-1}P_{JJ+1} & P_{JJ+1}^2 \end{pmatrix}\Delta_{LT}. \tag{4.7}$$

Therefore it is found immediately that $\mathbf{Q}_{JM}^{\rm surf}$ is an eigenstate having energy $E_J^{\rm surf}$.

By diagonalizing the matrix K we get T modes,

$$\mathbf{Q}_{JM}^{Tm}(\mathbf{r})=\sqrt{(J+1)(2J+1)}\sum_n f_{mnJ}\mathbf{Q}_{nJJ-1M}(\mathbf{r})$$
$$-\sqrt{\frac{J}{2J+1}}\mathbf{Q}_{mJJ+1M}(\mathbf{r}), \tag{4.8}$$

with energy $E^{Tm}=0$, and L modes,

$$\mathbf{Q}_{JM}^{Lm}(\mathbf{r})=\sqrt{J(2J+1)}\sum_n f_{mnJ}\mathbf{Q}_{nJJ-1M}(\mathbf{r})$$
$$-\sqrt{\frac{J+1}{2J+1}}\mathbf{Q}_{mJJ+1M}(\mathbf{r}), \tag{4.9}$$

with energy $E^{Lm}=\Delta_{LT}$. The divergence and rotation of the polarizations for these modes are obtained by using Eqs. (3.6) and (3.16) and Eq. (A9) in the Appendix. These modes are confirmed to be T or L mode as follows:

$$\nabla\cdot\mathbf{Q}_{JM}^{Tm}(\mathbf{r})=0,$$
$$\nabla\times\mathbf{Q}_{JM}^{Tm}(\mathbf{r})=i\sqrt{\frac{2}{a^3}}\frac{j_J(k_{mJ+1}r)}{j_J(\kappa_{mJ+1})}k_{mJ+1}\mathbf{Y}_{JM}(\hat{\mathbf{r}}),$$
$$\nabla\cdot\mathbf{Q}_{JM}^{Lm}(\mathbf{r})=\sqrt{\frac{2}{a^3}}\frac{j_J(k_{mJ+1}r)}{j_J(\kappa_{mJ+1})}k_{mJ+1}Y_{JM}(\hat{\mathbf{r}}), \tag{4.10}$$
$$\nabla\times\mathbf{Q}_{JM}^{Lm}(\mathbf{r})=0.$$

Both L and T modes are infinitely degenerate for each J while the S mode is a nondegenerate state. It is noted that the effect of the image potential does not appear in the L mode. This situation is also found for confined excitons having finite translational mass, and its demonstration will be given in the next section.

V. THE CASE OF FINITE MASS

A. Energy levels

For a finite translational mass of exciton, the level structure is obtained from numerical calculations, except for the pure L ($J=0$, $\ell=1$) and T ($J=\ell\geqslant 1$) modes discussed in Sec. III C. Figure 1 shows the energy levels of an exciton with $J=1$ as a function of radius. The relative dielectric constant $\epsilon_1/\epsilon_2=5.6$ corresponds to the situation in which an exciton is confined in a CuCl crystal and its surrounding is vacuum. The unit of radius $\hbar/\sqrt{2M_{\rm ex}\Delta_{LT}}$ is chosen as the de Broglie wavelength for a particle with mass $M_{\rm ex}$ and energy Δ_{LT}. In the upper abscissa the radius is converted using the parameter for the Z_3 exciton of CuCl, i.e., $\Delta_{LT}=5.7$ meV and $M_{\rm ex}=2.3m_e$. Although the number of basis in the calculation is only 29, the convergence is satisfied very well except for the isolated level corresponding to the S mode in the $M_{\rm ex}=\infty$ limit, whose energy lies between 0 and Δ_{LT}. If we increase the number of bases, the additional levels are piled above the highest level of each branch approaching L and T modes in the $M_{\rm ex}=\infty$ limit. In the figure, we can see how the discrete size-quantized levels approach the bulk L, T, and S modes.

Figure 2 gives the result for some lower levels as a function of the inverse square of radius. The solid lines show the lowest three levels with $J=1$, and the dotted and dashed lines show the lowest two levels of pure L and T modes, respectively. The levels of pure L and T modes are linear in the inverse square of radius and separated from each other by Δ_{LT} as shown in Sec. III C. It should be noted that the lowest $J=1$ level is isolated, while the higher members consist of a pair of levels with a splitting of the order of Δ_{LT}. Figure 3 shows the three lowest levels of $J=1$ together with the hy-

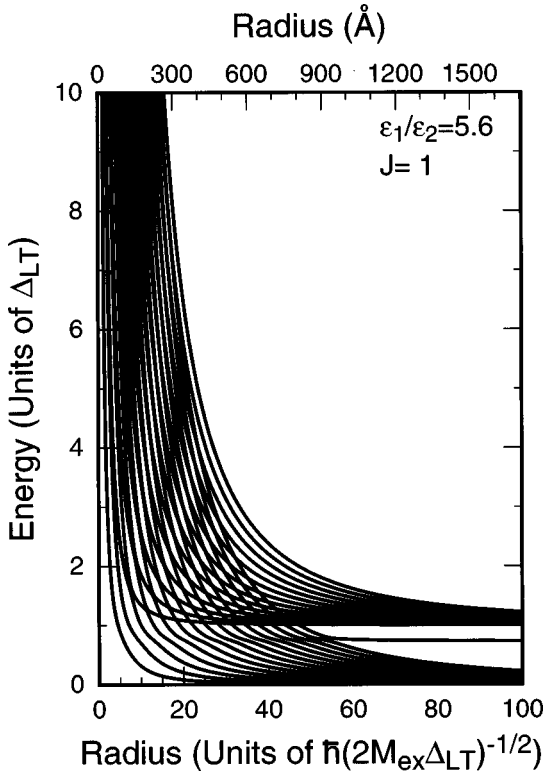

FIG. 1. Calculated energy levels of a confined exciton with $J=1$ as a function of radius of QD's. Levels for pure T ($\ell=1$) modes are not included. The radius unit $\hbar/\sqrt{2M_{\rm ex}\Delta_{LT}}$ is the de Broglie wavelength for Δ_{LT}. In the upper abscissa the radius is given in units of Å by using the parameter for the Z_3 exciton of CuCl, i.e., $\Delta_{LT}=5.7$ meV and $M_{\rm ex}=2.3m_e$.

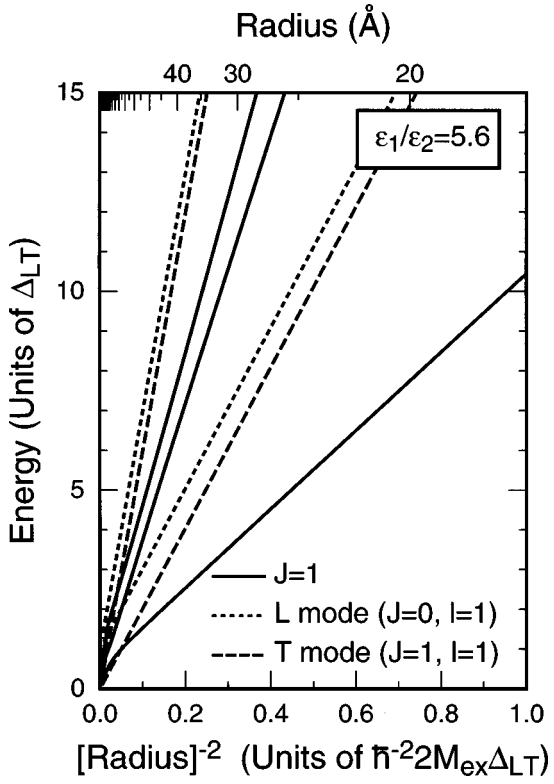

FIG. 2. Calculated lowest levels as a function of the inverse square of the radius.

pothetical levels of pure T modes ($\hbar^2k_{n0}^2/2M_{\rm ex}$) and pure L modes ($\hbar^2k_{n0}^2/2M_{\rm ex}+\Delta_{LT}$). The lowest and the third-lowest levels lie between the energies of L and T modes with $\ell=0$. The second-lowest level has energy between L and T modes with $\ell=2$ which are not shown in this figure. These results imply that exciton modes in a small sphere are LT mixed states except for the pure L and T modes, which will be explicitly shown in Figs. 6 and 7.

Figure 4 exhibits the energy levels of the exciton with $J=1$ as functions of radius. The curves of $\hbar^2k_{n0}^2/2M_{\rm ex}$ and $\hbar^2k_{n0}^2/2M_{\rm ex}+\Delta_{LT}$ are shown by dotted and dashed lines, respectively, which exhibit good agreement with the numerical calculation for sufficiently large spheres. However, one exception can be seen around the energy of the S mode in the $M_{\rm ex}=\infty$ limit, where the levels show crossover behavior. Every level gets an appreciable mixture of S modes in such a crossover region.

Figure 5 gives the energy levels of the $J=1$ exciton (solid lines) and those obtained by eliminating the image-potential part (dashed lines). As mentioned before, only the S mode is affected by the image potential in the $M_{\rm ex}=\infty$ limit, and in fact the energy of the isolated level corresponding to the S mode in the $M_{\rm ex}=\infty$ limit is shown to be increased appreciably due to the image potential. The image-potential effect also appear in the cross-over region having the S-like character. It should be noted that levels approaching the L mode are not affected by the image potential.

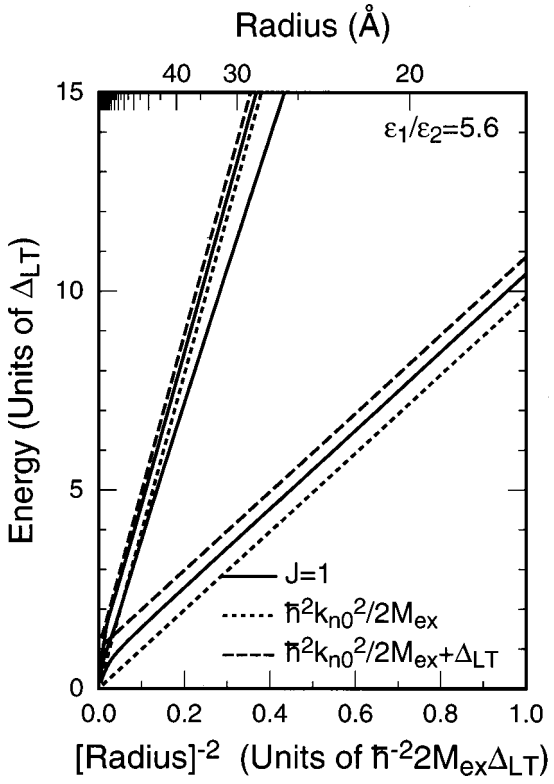

FIG. 3. Calculated three lowest levels with $J=1$ as a function of inverse square of the radius denoted by solid lines. Dotted and dashed lines represent hypothetical levels for L and T modes, respectively.

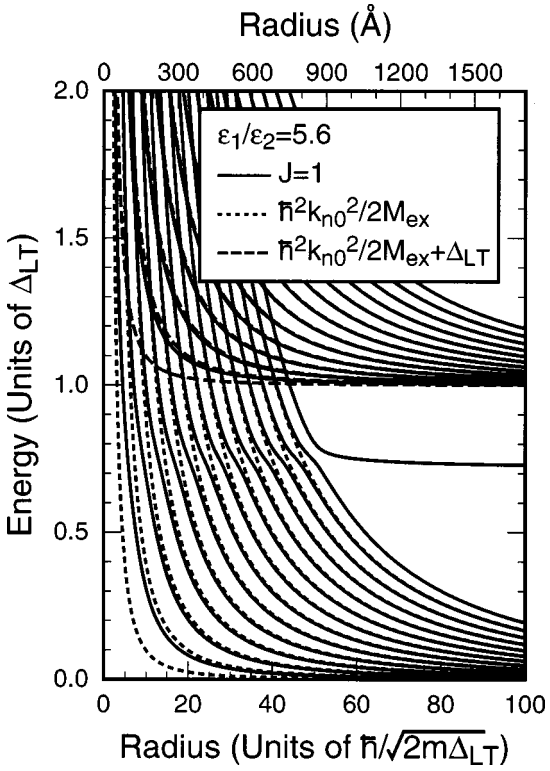

FIG. 4. Calculated energy levels as a function of radius denoted by solid lines. Dotted and dashed lines represent levels approximated by L and T modes, respectively.

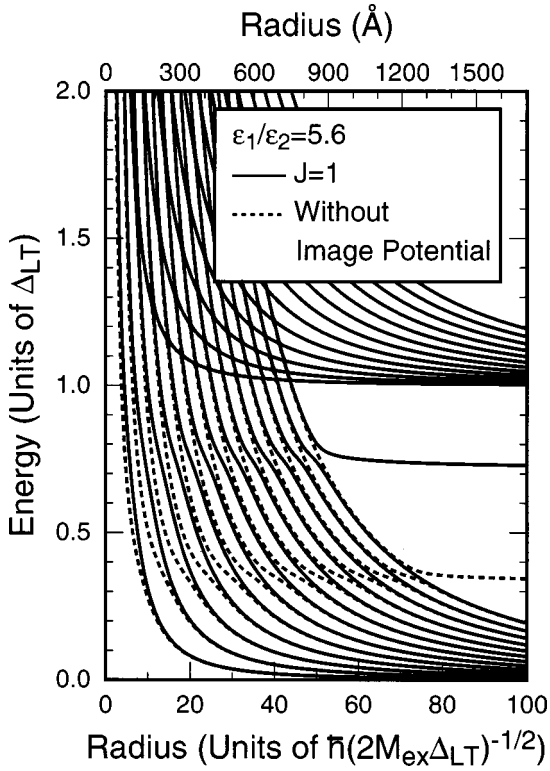

FIG. 5. Energy levels (solid lines) and those obtained by eliminating the image-potential part (dotted lines) are calculated as a function of radius.

It is demonstrated generally that the effect of the image potential does not appear in the L mode of an exciton confined in an arbitrary shape. We rewrite the Schrödinger equation (2.8) as

$$-\frac{\hbar^2}{2M_{\rm ex}}\nabla^2\mathbf{P}(\mathbf{r})-\frac{\epsilon_1\Delta_{LT}}{4\pi}\mathbf{E}(\mathbf{r})=E\mathbf{P}(\mathbf{r}), \tag{5.1}$$

where $\mathbf{E}(\mathbf{r})$ is a static electric field produced by the induced polarization charge as follows:

$$\mathbf{E}(\mathbf{r})=-\nabla\int d\mathbf{r}'\left[\frac{1}{\epsilon_1}\frac{1}{|\mathbf{r}-\mathbf{r}'|}+V_{\rm im}(\mathbf{r},\mathbf{r}')\right][-\nabla\cdot\mathbf{P}(\mathbf{r}')]. \tag{5.2}$$

When a polarization wave is the L mode, we have $\nabla^2\mathbf{P}=\nabla\nabla\cdot\mathbf{P}-\nabla\times\nabla\times\mathbf{P}=\nabla\nabla\cdot\mathbf{P}$. Taking the divergence of Eq. (5.2), we get an equation for the polarization charge

$$\left[-\frac{\hbar^2}{2M_{\rm ex}}\nabla^2+\Delta_{LT}\right]\nabla\cdot\mathbf{P}(\mathbf{r})=E\nabla\cdot\mathbf{P}(\mathbf{r}), \tag{5.3}$$

where we use the fact that the image potential satisfies the Laplace equation, i.e.,

$$\nabla^2\left[\frac{1}{\epsilon_1}\frac{1}{|\mathbf{r}-\mathbf{r}'|}+V_{\rm im}(\mathbf{r},\mathbf{r}')\right]=-\frac{4\pi}{\epsilon_1}\delta(\mathbf{r}-\mathbf{r}'). \tag{5.4}$$

Hence the equation $\nabla\cdot\mathbf{P}$ satisfies the Helmholtz equation $(\nabla^2+q^2)\nabla\cdot\mathbf{P}=0$, and we find the eigenenergy for the L mode to be $E=\hbar^2k^2/2M_{\rm ex}+\Delta_{LT}$, in which the effect of image potential does not appear. Note that we do not use the information of the confinement shape in the demonstration.

B. L and T components

Figure 6(b) exhibits $\int d\mathbf{r}|\mathrm{div}\,\mathbf{P}(\mathbf{r})|^2$ and 6(c) $\int d\mathbf{r}|\mathrm{rot}\,\mathbf{P}(\mathbf{r})|^2$ of the levels α, β, and γ, which approach the T mode in the large-radius limit as is shown in Fig. 6(a). The integration of the rotation is measured in units of that in the $M_{\rm ex}=\infty$ limit, i.e., $\int d\mathbf{r}|\mathrm{rot}\,\mathbf{P}_{JM}^{Tm}(\mathbf{r})|^2=\kappa_{mJ+1}^2(|\mu|^2/a^2)$. Sharp peaks in Fig. 6(b) and dips in Fig. 6(c) occur at the radii where the levels β and γ cross the levels approaching the L mode. In the level α the divergence decreases with radius and becomes zero. On the other hand the rotation increases with radius and reaches the same value as that in the $M_{\rm ex}=\infty$ limit. Therefore we conclude that the level α is a LT mixed mode in sufficiently small QD's, which becomes a T mode with an increase of radius. Similarly the other levels approaching T modes are LT mixed modes for small QD's.

Vertical arrows denote the radii where each level crosses the energy of the S mode in the $M_{\rm ex}=\infty$ limit. Around the radii indicated by the arrows the divergence and rotation show the local maximum and local minimum, respectively. This comes from the fact that T and S modes are coupled in the crossover region.

Figure 7(b) shows $\int d\mathbf{r}|\mathrm{div}\,\mathbf{P}(\mathbf{r})|^2$ and 7(c) $\int d\mathbf{r}|\mathrm{rot}\,\mathbf{P}(\mathbf{r})|^2$ of the levels ρ, σ, and τ in Fig. 7(a), which approach the L mode in the large-radius limit. The integration of divergence is measured in units of that in the $M_{\rm ex}=\infty$ limit, i.e., $\int d\mathbf{r}|\mathrm{div}\,\mathbf{P}_{JM}^{Lm}(\mathbf{r})|^2=\kappa_{mJ+1}^2(|\mu|^2/a^2)$. For each level the divergence is less than that of the L mode and the rotation also takes a finite value, and thus each level is a LT mixed mode. With an increase of radius these levels get more L-mode

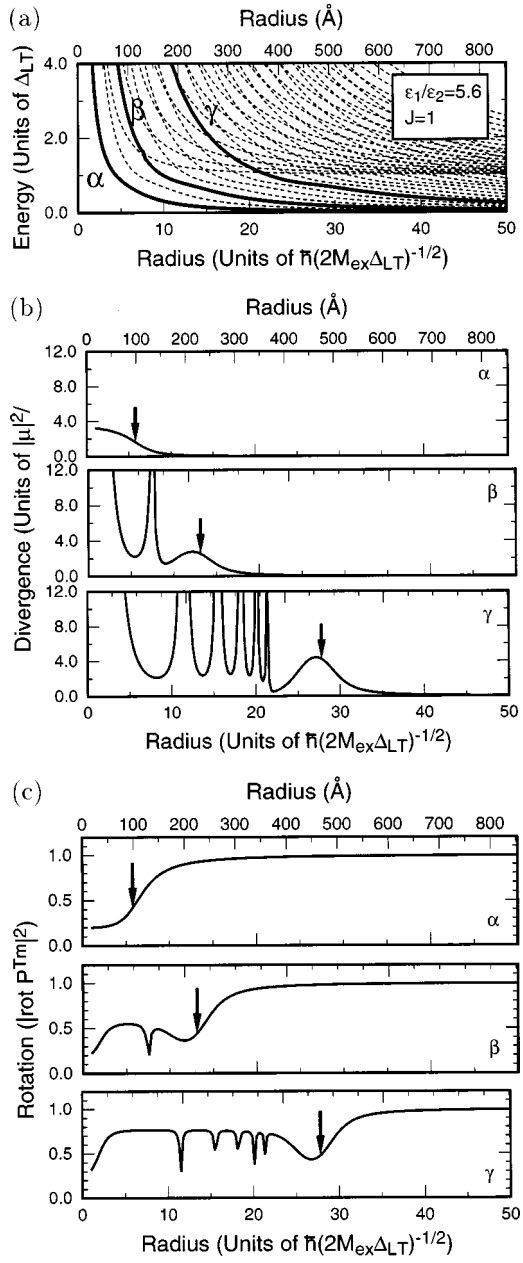

FIG. 6. (a) Energy levels indicated by α, β, and γ that approach T modes in the infinite-mass limit. (b) Calculated L component $[\int d\mathbf{r}|\mathrm{div}\,\mathbf{P}(\mathbf{r})|^2]$ of levels α, β, and γ as a function of radius. (c) Calculated T component $[\int d\mathbf{r}|\mathrm{rot}\,\mathbf{P}(\mathbf{r})|^2]$ of levels α, β, and γ as a function of radius. Vertical arrows indicate radii where each level crosses the energy of the S mode in the infinite-mass limit.

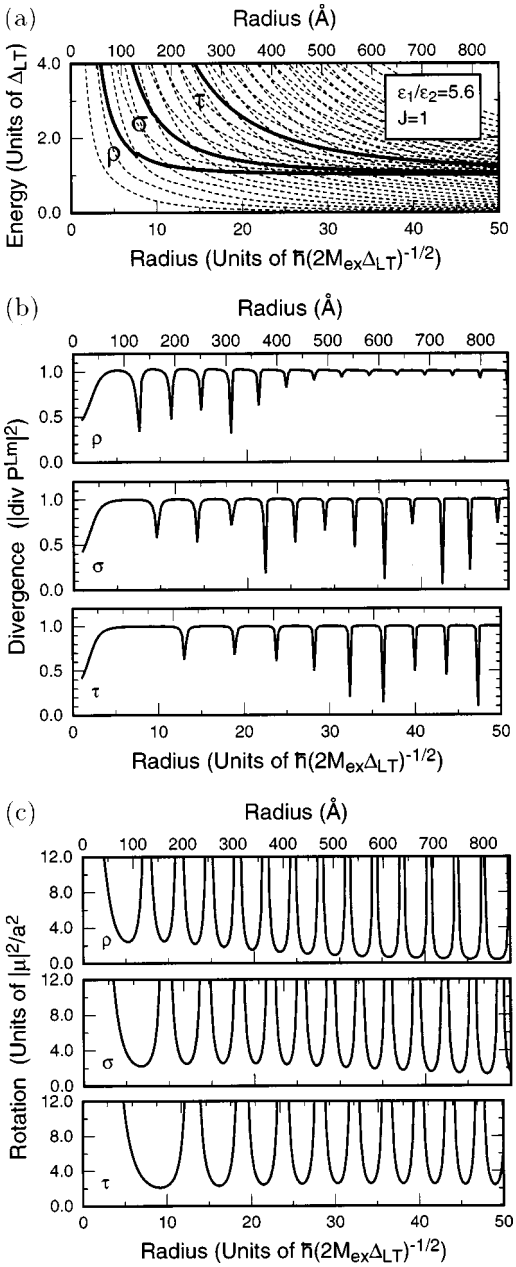

FIG. 7. (a) Energy levels indicated by ρ, σ, and τ, which approach L des in the infinite-mass limit. (b) Calculated L component $[\int d\mathbf{r}|\mathrm{div}\,\mathbf{P}(\mathbf{r})|^2]$ of levels ρ, σ, and τ as a function of radius. (c) Calculated T component $[\int d\mathbf{r}|\mathrm{rot}\,\mathbf{P}(\mathbf{r})|^2]$ of levels ρ, σ, and τ as a function of radius.

character except for the crossing regions, where sharp dips in Fig. 7(b) and peaks in Fig. 7(c) appear.

C. Oscillator strength

In the long-wavelength approximation (LWA), the one-photon transition is characterized by oscillator strength. The oscillator strength per unit volume of the nth-level exciton is given by[32]

$$f_{JM}^{n}=\frac{2\omega_{JM}^{n}m_0}{\hbar e^2}\frac{1}{V_0}\left|\int d\mathbf{r}\,\mathbf{P}_{JM}^{n}(\mathbf{r})\right|^2, \tag{5.5}$$

where $\mathbf{P}_{JM}^{n}$ is the polarization mode of the nth level, $\hbar\omega_{JM}^{n}$ is the excitation energy, and V_0 is the volume of the sphere. Only the component with $\ell=0$ takes a finite value from the integration of the angular part of $\mathbf{Q}_{JM}^{n}(\mathbf{r})$. Therefore the optical transition is allowed only for $J=1$, and thus the transitions to pure L $(J=0,\ \ell=1)$ and T $(J=\ell\geqslant 1)$ modes are forbidden for one-photon transitions within the LWA. The oscillator strength of the exciton with $J=1$ can be rewritten as

$$f_{1M}^{n}=6\left|\sum_m\frac{C_{m0}^{n}}{\kappa_{m0}}\right|^2 f_{\mathrm{bulk}}, \tag{5.6}$$

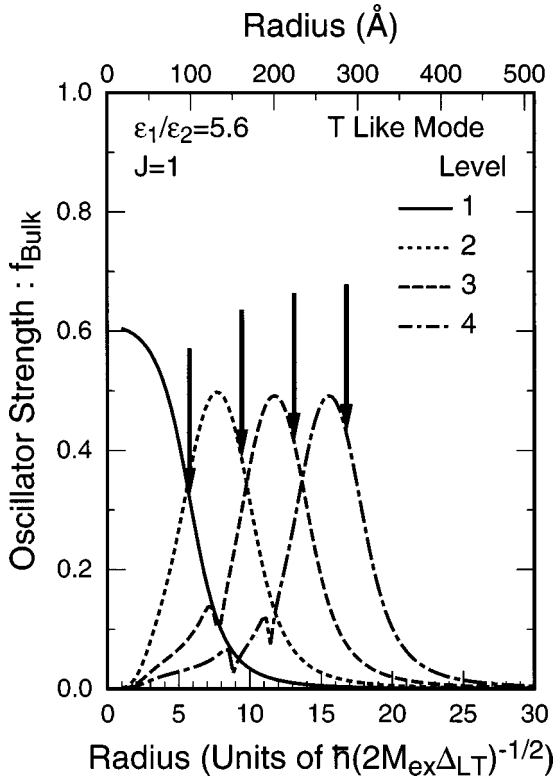

FIG. 8. Calculated oscillator strength per unit volume for the lowest four levels approaching T modes as a function of radius. Vertical arrows denote the radii in which each level cross the energy of the S mode in the infinite-mass limit.

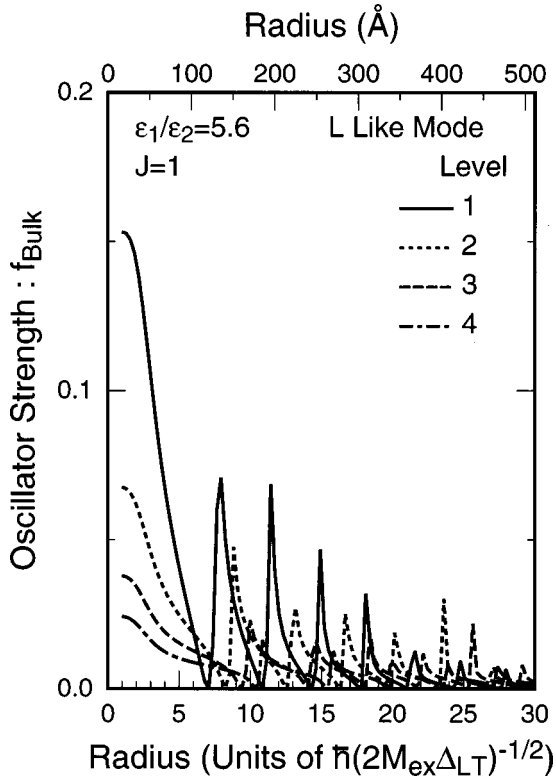

FIG. 9. Calculated oscillator strength per unit volume for the lowest four levels approaching L modes as a function of radius.

where $C^n_{m\ell}$ is the expansion coefficients of the nth level with bases $\mathbf{Q}_{mJ\ell M}$, and $f_{\rm bulk}=2\omega_0 m_0/\hbar e^2$ is the oscillator strength per unit volume for a bulk crystal. The sum rule of the oscillator strength is confirmed in the numerical calculation, and for instance, it becomes about $0.976 f_{\rm bulk}$ if the number of basis is 50.

Figure 8 shows the calculated oscillator strength per unit volume for various levels from the lowest (solid line) to the fourth-lowest (dash-dotted line) ones approaching T modes as a function of radius. For small radii, the oscillator strength is concentrated on the lowest level, and, as the radius increases, it starts to decrease and eventually vanishes. The vertical arrows show the radii where the levels cross the energy of the S mode in the $M_{\rm ex}=\infty$ limit, and it is found that the oscillator strength of the level 2, 3, or 4 takes a maximum around the energy of the S mode. This result agrees with the theoretical analysis in the LWA by Ekimov *et al.*[18]

Figure 9 shows the oscillator strength per unit volume for various levels from the lowest (solid line) to the fourth-lowest (dash-dotted line) ones approaching L modes as a function of radius. Since these levels are LT mixed modes, the oscillator strengths take finite values. With an increase of radius the oscillator strengths decrease because the levels approach pure L modes as shown in Fig. 7.

VI. SUMMARY AND CONCLUSION

The energies and mode character of the excitons confined in a sphere have been calculated in a weak-confinement regime, including the e-h exchange interaction and image-potential energy. It is found that the states ($J=0, \ell=1$) and ($J=\ell$) and L and T modes, respectively, independent of radius. The other states are LT mixed modes, and with the increase of radius they approach L, T, and S modes, which are in agreement with those obtained analytically in the $M_{\rm ex}=\infty$ limit. The effect of the image potential manifests itself mainly at the crossover region around the energy of the S mode in the $M_{\rm ex}=\infty$ limit.

We have also studied the oscillator strength per unit volume, which is meaningful only when the LWA is valid. For sufficiently small radii (up to about 100 Å in the case of the Z_3 exciton in CuCl) the lowest level has the largest oscillator strength and the states approaching the L mode take still finite values. It is also found that the oscillator strength becomes maximum around the S mode in agreement with the analysis by Ekimov *et al.*

ACKNOWLEDGMENTS

We would like to thank Professor H. Ishihara and Mr. J. Ushida for useful discussions. Numerical calculations were performed in part on FACOM VPP500 in Supercomputer Center, Institute for Solid State Physics, University of Tokyo. This work was supported in part by Grant-in-Aid for COE Research (10CE2004) of the Ministry of Education, Science, Sports and Culture of Japan, and also by the Mitsubishi Foundation.

APPENDIX: FORMULAS FOR SUMMATIONS OF INFINITE SERIES

The orthonormality of the polarization vector of L, T, and S modes in the $M_{\rm ex}=0$ limit given in Eqs. (4.4), (4.8), and (4.9) is confirmed by using of the following formulas:

$$\sum_{n=1}^{\infty} \frac{1}{\kappa_{nJ-1}^2} = \frac{1}{2(2J+1)}, \tag{A1}$$

$$\sum_{n=1}^{\infty} \frac{1}{\kappa_{mJ+1}^2 - \kappa_{nJ-1}^2} = -\frac{1}{2\kappa_{mJ+1}} \frac{j_J(\kappa_{mJ+1})}{j_{J-1}(\kappa_{mJ+1})}, \tag{A2}$$

$$\sum_{n=1}^{\infty} \frac{1}{\kappa_{mJ+1}^2 - \kappa_{nJ-1}^2} \frac{1}{\kappa_{m'J+1}^2 - \kappa_{nJ-1}^2} = 0 \quad (m \neq m'), \tag{A3}$$

$$\sum_{n=1}^{\infty} \frac{1}{(\kappa_{mJ+1}^2 - \kappa_{nJ-1}^2)^2} = \frac{1}{4(2J+1)^2}. \tag{A4}$$

We shall prove the above formulas. We consider the sequence of contour integrals along C_n,

$$I_n = \frac{1}{2\pi i} \oint_{C_n} d\zeta \frac{1}{\zeta(\zeta - z)} \frac{j_J(z)}{j_{J-1}(z)}, \tag{A5}$$

where C_n represents the circular path about origin including zeros of $j_{J-1}(z)$, $\pm\kappa_{1J-1},\ldots,\pm\kappa_{nJ-1}$, and not passing through any other zeros, and z is any point inside C_n other than zeros. A residue integration gives

$$I_n = \frac{1}{z} \frac{j_J(0)}{j_{J-1}(0)} - \frac{1}{z} \frac{j_J(z)}{j_{J-1}(z)} + \sum_{m=1}^{n} \left[\frac{1}{\kappa_{mJ-1}(z - \kappa_{mJ-1})} - \frac{1}{\kappa_{mJ-1}(z + \kappa_{mJ-1})} \right]. \tag{A6}$$

Because of $\lim_{n\to\infty} I_n = 0$ we finally obtain

$$\sum_{n=1}^{\infty} \frac{1}{z^2 - \kappa_{nJ-1}^2} = -\frac{1}{2z} \frac{j_J(z)}{j_{J-1}(z)}. \tag{A7}$$

Substituting $z=0$ and $z=\kappa_{mJ+1}$, we have Eqs. (A1) and (A2), respectively. Formulas Eqs. (A3) and (A4) can be also obtained in a similar way using contour integral

$$I_n' = \frac{1}{2\pi i} \oint_{C_n} d\zeta \frac{1}{\zeta(\zeta - z_1)(\zeta - z_2)} \frac{j_J(z)}{j_{J-1}(z)}. \tag{A8}$$

In the calculation of the divergence and the rotation for the polarization vector of L, T, and S modes, we have a useful formula:

$$\sum_{n=1}^{\infty} \frac{1}{\kappa_{mJ+1}^2 - \kappa_{nJ-1}^2} \frac{j_J(\kappa_{nJ-1}x)}{j_J(\kappa_{nJ-1})} = -\frac{1}{2\kappa_{mJ+1}} \frac{j_J(\kappa_{mJ+1}x)}{j_{J-1}(\kappa_{mJ+1})} \quad (0 \leqslant x \leqslant 1). \tag{A9}$$

This is obtained from a sequence of contour integrals

$$I_n'' = \frac{1}{2\pi i} \oint_{C_n} d\zeta \frac{1}{\zeta(\zeta - z)} \frac{j_J(zx)}{j_{J-1}(z)}. \tag{A10}$$

[1] A. I. Ekimov and A. A. Onushchenko, Fiz. Tekh. Poluprovodn. **16**, 1215 (1982) [Sov. Phys. Semicond. **16**, 775 (1982)].
[2] A. I. Ekimov, AI. L. Efros, and A. A. Onushchenko, Solid State Commun. **56**, 921 (1985).
[3] S. Nagasaka, M. Ikezawa, and M. Ueta, J. Phys. Soc. Jpn. **20**, 1540 (1965).
[4] H. Kishishita, Phys. Status Solidi B **55**, 399 (1973).
[5] T. Tsuboi, J. Chem. Phys. **72**, 5343 (1980).
[6] T. Itoh and K. Kirihara, J. Lumin. **31/32**, 120 (1984).
[7] C. Zaldo and F. Jaque, J. Phys. Chem. Solids **46**, 689 (1984).
[8] T. Itoh, Y. Iwabuchi, and M. Kataoka, Phys. Status Solidi B **145**, 567 (1988).
[9] T. Itoh, Y. Iwabuchi, and T. Kirihara, Phys. Status Solidi B **146**, 531 (1988).
[10] Al. L. Efros and A. L. Efros, Fiz. Tekh. Poluprovodn. **16**, 1209 (1982) [Sov. Phys. Semicond. **16**, 772 (1982)].
[11] L. E. Brus, J. Chem. Phys. **80**, 4403 (1984).
[12] H. M. Schmidt and H. Weller, Chem. Phys. Lett. **129**, 615 (1986).
[13] Y. Kayanuma, Solid State Commun. **59**, 405 (1986).
[14] S. V. Nair, S. Sinha, and K. C. Rustagi, Solid State Commun. **59**, 405 (1986).
[15] Y. Kayanuma, Phys. Rev. B **38**, 9797 (1988).
[16] T. Takagahara, Phys. Rev. B **47**, 4569 (1993).
[17] A. V. Baranov, Y. Masumoto, K. Inoue, A. V. Fedorov, and A. A. Onushchenko, Phys. Rev. B **55**, 15 675 (1997).
[18] A. I. Ekimov, A. A. Onushchenko, M. E. Raikh, and Al. L. Efros, Zh. Eksp. Teor. Fiz. **90**, 1795 (1986) [Sov. Phys. JETP **63**, 1054 (1986)].
[19] R. Ruppin, J. Phys. Chem. Solids **50**, 877 (1989).
[20] S. V. Goupalov and E. L. Ivchenko, J. Cryst. Growth **184/185**, 393 (1998).
[21] K. Cho, J. Phys. Soc. Jpn. **68**, 683 (1999).
[22] K. Cho, M. Nishida, Y. Ohfuti, and L. Belleguie, J. Lumin. **60/61**, 330 (1994).
[23] K. Cho, Prog. Theor. Phys. Suppl. **106**, 225 (1991).
[24] Y. Ohfuti and K. Cho, Phys. Rev. B **52**, 4828 (1995); J. Lumin. **66/67**, 94(E) (1996).
[25] K. Cho, J. Phys. Soc. Jpn. **66**, 2496 (1997).
[26] H. Ajiki and K. Cho, in *Proceedings of the Third International Conference on Excitonic Processes in Condensed Matter, Boston, 1998*, edited by R. T. Willians and W. M. Yen (Electrochemical Society, Pennington, NJ, 1999), p. 262.
[27] W. R. Heller and A. Marcus, Phys. Rev. **84**, 809 (1951).
[28] Y. Onodera and Y. Toyozawa, J. Phys. Soc. Jpn. **22**, 833 (1967).
[29] K. Cho, in *Proceedings of the 14th International Conference on Physics of Semiconductors, Bristol and London, 1978*, edited by B. L. H. Wilson (IOP, Bristol, 1979), p. 841.
[30] A. R. Edomonds, *Angular Momentum in Quantum Mechanics* (Princeton University Press, Princeton, NJ, 1996), p. 81.
[31] M. C. Klein, F. Hache, D. Ricard, and C. Flytzanis, Phys. Rev. B **42**, 11 123 (1990).
[32] C. H. Henry and K. Nassau, Phys. Rev. B **1**, 1628 (1970).